

# Camera Based Full-Field Laser Interferometric Vibrometry for Combustion Diagnostics

Felix Greiffenhagen<sup>1\*</sup>, Jakob Woisetschläger<sup>1</sup>,  
Johannes Gürtler<sup>2</sup>, Robert Kuschmierz<sup>2</sup>, Jürgen Czarske<sup>2</sup>

1: Institute for Thermal Turbomachinery and Machine Dynamics, Graz University of Technology, 8010 Graz, Austria

2: Laboratory for Measurement and Sensor System Techniques, TU Dresden, 01069 Dresden, Germany

\* Correspondent author: felix.greiffenhagen@tugraz.at

**Keywords:** interferometry, laser vibrometry, thermoacoustics, combustion diagnostics, high-speed camera

## ABSTRACT

Laser Interferometric Vibrometry (LIV) is well suited to detect fluctuations in heat release rate globally and locally. Modern combustion concepts in turbomachinery focus on lean and premixed, swirl stabilized flames, prone to thermo-acoustic instabilities. This type of flame is characterized by the Flame Transfer Function (FTF), which relates flow oscillations at the burner exit to global fluctuations of the heat release rate. FTFs are plotted as function of frequency, to identify critical operation points with respect to thermo-acoustic instabilities. To speed up such a recording of a FTF, we present a full-field or camera-based LIV (CLIV), recording the local heat release fluctuation rate for each frequency within seconds. Instantaneous recordings and the sound emission from such a flame are also discussed. The data are compared to global chemiluminescence recordings performed with a photomultiplier.

---

## 1. Introduction

Combustion noise caused by fluctuations in heat release is not only considered as a pollutant, but can also cause combustion instabilities, which in the worst case can lead to malfunction or damage of turbomachinery. Modern combustion concepts with lean and premixed, swirl stabilized flames, targeting towards lower temperature and therefore low NO<sub>x</sub>, are more vulnerable to instabilities due to reduced core mass flow and damping capabilities (Dowling and Mahmoudi 2015). The determination of those fluctuations is usually done with CH\* or OH\* radical chemiluminescence or Planar Laser Induced Fluorescence (PLIF). Balachandran et al. (2005) confirms that chemiluminescence is a trusted tool for determining the global heat release fluctuations (volume integral of fluctuations). Lauer (2011) recommended to carefully interpret chemiluminescence data, especially local resolved data should be taken with care, since mixture gradients and strain rate influence the local emission of radicals.

Since variations of heat release leads to variations in density, Laser Interferometric Vibrometry (LIV) came into play. LIV is a line-of-sight technique, directly recording density

fluctuations along the laser beam axis in unconfined, as well as in confined flames (Giuliani et al 2006, Leitgeb et al. 2013, Peterleithner et al. 2016a). Local data can be obtained from the integral ones by methods of tomography or Abel inversion. Recently it was shown, that LIV is capable to predict density fluctuations quantitatively (Greiffenhagen et al. 2017). A not yet published work from the authors of this paper also showed a good match of the global data when LIV and chemiluminescence recordings are compared (Greiffenhagen et al. 2018). Up to now, commercially available LIV-systems were used, originally designed to measure surface vibrations without mechanical contact. Those LIVs are only capable to measure in a single position, time consuming traversing of the flame is necessary to obtain full field data. Such a scan can take several hours, a fact that may lead to problems if the combustion system is not stable for such a long measurement period. To overcome this, the target of the Austrian-German joint research project “Full-field laser vibrometry for combustion diagnostics” funded by the Austrian FWF and the German DFG is to develop a planar, camera based full-field LIV system. This system is capable to record the whole combustion field within a single measurement, by forming an interference pattern between an object- and a reference beam on a high speed camera. Also the recording of unsteady data is possible with this system.

In this work, the Camera based LIV (CLIV) is used to record an Flame Transfer Function (FTF) of a swirl-stabilized flame as used in turbomachinery combustion, but at lower power and under atmospheric conditions. A FTF is used to classify the flame in terms of its frequency response and relates the global heat release fluctuations to the incoming velocity fluctuations in amplitude and phase, both at a given frequency (Candel et al. 2014). Such a frequency scan is time-consuming when a LIV has to scan the flame field for each frequency (Peterleithner et al. 2016b). Here the process speeds up significantly when a full-field LIV is used.

## 2. Theoretical background – recording heat release fluctuations by detecting density fluctuations

LIV technique records density fluctuations. For combustion diagnostics density fluctuations have to be linked to heat release fluctuations. In this section we will briefly discuss the assumptions that lead to such a direct relationship. Starting with the energy equation, considering a reactive gas, consisting of  $N$  species (Williams 1994), and neglecting body forces (Lieuwen 2012, Crighton et al. 1992), the energy equation can be written in terms of density fluctuations:

$$\frac{d\rho}{dt} = \frac{1}{c^2} \frac{dp}{dt} + \frac{(\kappa - 1)\rho}{\kappa p} \left\{ \left( \sum_{n=1}^N \frac{\partial h}{\partial Y_n} \Big|_{T,p,Y_m} - \frac{\partial h}{\partial \rho} \Big|_{p,Y_m} \sum_{n=1}^N \frac{\partial \rho}{\partial Y_n} \Big|_{T,p,Y_m} \right) \rho \frac{dY_n}{dt} + \nabla \mathbf{q} - \frac{\partial u_i}{\partial x_j} \tau_{ij} \right\} \quad (1)$$

With  $\rho$  the density,  $\kappa$  the ratio of heat capacities,  $c$  the speed of sound and pressure  $p$ . The first term on the right side indicates the influence of pressure on density. It has already been shown, that pressure changes caused by sound waves or turbulence can be visualized in an isothermal flow by interferometric measurements (Martarelli et al. 2013, Gren et al 2006, Zipser et al 2002, Mayrhofer and Woisetschlager 2001). The term  $\rho \frac{dY_n}{dt} = \omega_n - \nabla \cdot \mathbf{J}_n$  is equal to the production of the  $n$ th species and its flux  $\mathbf{J}_n$  by diffusion. When diffusion is neglected, the first summation in the second term on the right side describes the rate of heat release per unit volume due to chemical reaction, with  $Y_m \neq n$  meaning, that there is no contribution from other molecules in each summation loop. The second summation term describes the change of density due to changes of species concentration at constant temperature and pressure. When burning hydrocarbons with air, this term is small compared to the heat release and therefore can be neglected, since the average molar mass is nearly constant (Crighton et al. 1996), due to the dilution of the reactive species with inert nitrogen (Lieuwen 2012). In oxy-combustion this term has to be considered.  $\nabla \cdot \mathbf{q}$  represents the heat flux due to conduction, convection and radiation. The last part  $\frac{\partial u_i}{\partial x_j} \tau_{ij}$ , with  $\tau_{ij}$ , the viscous stress tensor and the flow velocities  $u_i$  defines the heat addition from friction. While the contribution from friction is small, heat flux by radiation and conduction to the walls might be significant. The swirl-stabilized flame used in this work, showed losses by radiation of 5% of the total thermal power (recorded by a thermopile). Since the flame was unconfined, there is no conduction of heat to solid walls.

In the flame volume, the pressure fluctuations in the combustion region are two orders of magnitude smaller than the amplitudes of heat release fluctuations. Therefore the following equation relates heat release fluctuations and density fluctuations in the flame:

$$\left. \frac{d\rho'}{dt} \right|_{p' \ll q_v'} = - \frac{(\kappa - 1)\rho}{\kappa p} \frac{\partial q_v'}{\partial t} \quad (2)$$

with  $q_v'$ , the volumetric heat release fluctuations and  $\frac{dq'_{flame,v}}{dt}$  the density fluctuations detect by LIV in the flame. Downstream of the flame, no chemical reactions take place but heat is convected by the flow. Thus, pressure waves will contribute to the fluctuations too. In this region, the density fluctuations can be described as:

$$\frac{d\rho'}{dt} = \frac{1}{c^2} \frac{dp'}{dt} - \frac{(\kappa - 1)\rho}{\kappa p} \frac{dq_v'}{dt} \quad (3)$$

Beside the flame, where no reaction and no convection of heat occurs, density changes are caused by sound waves:

$$\left. \frac{d\rho'}{dt} \right|_{T, q_v} = \frac{1}{c^2} \frac{dp'}{dt} \quad (4)$$

With fluctuations ( $\rho'$ ) and steady state ( $\bar{\rho}$ ) variables we obtain the following relation from eq. 2:

$$\left. \frac{1}{\bar{\rho} + \rho'} \frac{d\rho'}{dt} \right|_{p' \ll q_v'} = - \frac{\bar{\kappa} - 1}{\bar{\rho} \bar{\kappa}} \frac{dq_v'}{dt} \quad (5)$$

From eq. 5 we learn that not only the density fluctuations  $\rho'$  must be recorded by LIV, but also the local density distribution  $\bar{\rho}$  must be measured. So, it is necessary to use another optical technique such as shearography, digital holography or background-oriented Schlieren to detect absolute density quantitatively. We used shearography (Pretzler et al 1993). While pressure fluctuations  $p'$  are small in all parts of the flame compared to the ambient pressure or the pressure in a combustion chamber  $\bar{p}$ , the local behavior of  $\bar{\kappa} + \kappa'$  is more complex to estimate and has to be done from experimental data. Using the ideal gas equation, fluctuations in temperature can be linked to fluctuations in density:  $dT = -T d\rho/\rho$ . Knowing these density data from interferometric measurements we find that the swirl-stabilized unconfined Methane flame discussed in this publication has a maximum temperature fluctuation amplitude of 22K, with average temperature fluctuations of 5.7K. The change of heat capacities over time is therefore small, what leads to eq. 5 as basic equation for our measurements.

When passing through any fluid flow, light interacts with the molecules present, resulting in a delayed wave front. This relationship finds its expression in the refractive index  $n$ , linked to the density by the Gladstone-Dale constant  $G$  (Merzkirch 1987, Gardiner et al. 1981):

$$n(x, y, z, t) - 1 = \rho(x, y, z, t) G \quad (6)$$

LIV is a line-of-sight measurement, meaning the quantity  $n$  is integrated along the laser beam axis:

$$L(t) = \int_l n(x, y, z, t) dz \quad (7)$$

with  $L$  the optical path. By interfering the object beam and an internal reference beam, LIVs detect changes of the optical path  $L$ . The intensity pattern seen on the detector is a function of the phase difference  $\Delta\varphi$  between object and reference beam, which can be related to the variation of the optical path, caused by the density fluctuations. The LIV principle uses a Mach-Zehnder type interferometer and a frequency modulation  $f_B$  by acousto-optical modulators (Bragg-cells) in the reference beam (e.g. Lewin et al. 1998). So, without any changes in optical path the interference pattern is modulated by this carrier frequency:

$$I(f_B, t) = \frac{I_0}{2} (1 + \cos(2\pi(f_B)t)) \quad (8)$$

When the optical path changes, these fluctuations in optical path modulate the carrier frequency. This modulation frequency can be expressed as  $\pm f_D = \frac{2u}{\lambda}$  (Doppler-effect) where  $u$  is the “velocity” of the object (or  $dL/dt$ ). Now eq. 8 changes to

$$I(\Delta f, t) = \frac{I_0}{2} (1 + \cos(2\pi(f_B \pm f_D)t)) \quad (9)$$

Thus, the modulation frequency  $\pm f_D$  provides the information on the fluctuations in optical path and therefore in density:

$$f_D = \frac{2}{\lambda} \frac{dL}{dt} = \frac{2}{\lambda} G \int_l \frac{d}{dt} \rho(t) dz \quad (10)$$

The sign of the Doppler shift is determined by the direction of the density fluctuations, related to the heat release fluctuations by eq. 5. In this configuration it is possible to detect refractive index (density) changes with respect to their sign or direction of motion with sub-nanometer resolution (Lewin 1998).

When relating the refractive index to density with the Gladstone-Dale constant in a reactive medium, one has to take care about the influence of the species concentrations on  $G$ . The Gladstone-Dale constant in general is only weakly dispersive and not dependent on temperature or pressure but on the type of species and its individual mass fraction. This means, that especially in non-premixed combustion, where equivalence ratio waves can occur, the local and time resolved equivalence ratio  $\Phi$  in the reaction zone has to be known to calculate a local Gladstone-Dale constant. To obtain local density information, tomographic algorithms must be applied to the line-of-sight data. In case of an axisymmetric flame, a single projection can be used to reconstruct the local field by Abel transform (Pretzler et al. 1992).

### 3. Camera-based full-field laser interferometric vibrometry (CLIV)

With commercial LIV systems, time consuming traversing through the entire volume is required, assuming steady state flame behavior. To reduce the measurement time and detect transient behavior of the flame, an instantaneous planar measurement of the heat release rate was realized by constructing a camera-based laser vibrometer (CLIV, Gürtler et al. 2016, Fig. 1). Here, a spatial resolution of 1mm is to be achieved, and resulting from the size of the combustion zone, a minimum image resolution of the camera of 50x50 px is needed, wherein each pixel enables integral detection of the heat release.

In addition to the requirement for the local resolution, there are demands on the measuring rate of the system. According to eqs. 10 and 5, the fluctuation of heat release rate results in a fluctuation of the Doppler frequency. This frequency fluctuation can be obtained from the time signal of the intensity measured by a camera pixel. In this case, the maximum possible measuring rate is limited by the frame rate  $f_K$  of the camera, since the intensity signal must be sampled in accordance with the Nyquist theorem and

$$f_K > 2(f_B + f_D) \quad (11)$$

in addition, the choice of the carrier frequency  $f_B$  must be taken into account. It determines the measuring range for the Doppler frequency (Selbach et al., 1992). Based on earlier measurements on the flame under investigation,  $f_D$  varies between a few kHz and up to 15 kHz (Peterleithner and Woisetschlager 2015). However, a carrier frequency  $f_B = 60$  kHz was chosen for the present design in order to achieve an extended measuring range for further investigations. The setup of the camera-based LIV is sketched in Fig. 1. The carrier frequency is realized by a cascade of two parallel-arranged acousto-optical modulators (AOM), wherein the dependence of the frequency shift on the direction of incidence of the laser beam is utilized. AOM 1 is operated at the center frequency  $f_c = 200$  MHz and AOM 2 with the frequency  $(f_c - f_B)$ , so that after passing through both AOMs the carrier frequency  $f_B$  modulates the laser frequency. For the scanning of the intensity signal, a high-speed camera "Phantom v1610" from Vision Research is used. The camera offers a maximum frame rate of 1 MHz with a resolution of 128x16px and a pixel size of 28  $\mu$ m. To safely meet the imposed local resolution requirement, a camera resolution of 110x110px is used, similar to an array of 12100 individual LIVs. Resulting in a reduced frame rate of 200 kHz, with eq. 11 satisfied for the entire measurement area. In addition, the measurement signal must be separated from the emitted flame light. For this purpose, a narrowband laser (Cobolt Samba 532) with a wavelength of  $\lambda = 532$  nm and a bandpass filter in front of the camera is used. The intensity profile detected by the camera is then evaluated for each pixel and the Doppler frequency is determined by means of Quadrature Demodulation Technique (QDT). Due to the high data rate, the total measurement time of 27s was divided into three measurements with nine seconds each, the maximum the high speed camera is able to record at once. To ease alignment and reduce losses and cross-talk between the pixels due to refraction by the density gradients in the flame, the system was set up in transmission with the laser beam passing the measurement volume only once. Thus, with a collimated lens system as shown in Fig. 1, a change of angle in the beam path caused by refraction, led to a change of angle on the image sensor, but not to a change of position on the sensor, avoiding cross-talk between the pixels. A benchmarking of the system using a loud speaker and the swirl-stabilized flame is provided by Gurtler et al. (2016) and (2017).

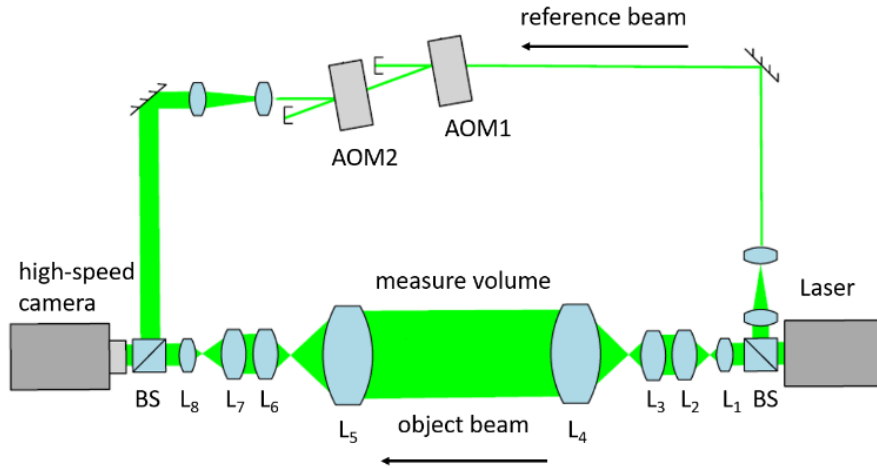


**Fig. 1:** CLIV in a transmissive setup: the laser beam is split up into an object beam and a reference beam (BS beam splitter). The object beam was expanded with lens 1 (L1) - lens 4 (L4) to a diameter of 71mm and bundled again (L5-L8) after the measure volume, while the reference beam is guided around the flame and modulated with Acousto-Optical Modulators (AOM 1,2). Both beams interfere at the image sensor of a high-speed camera.

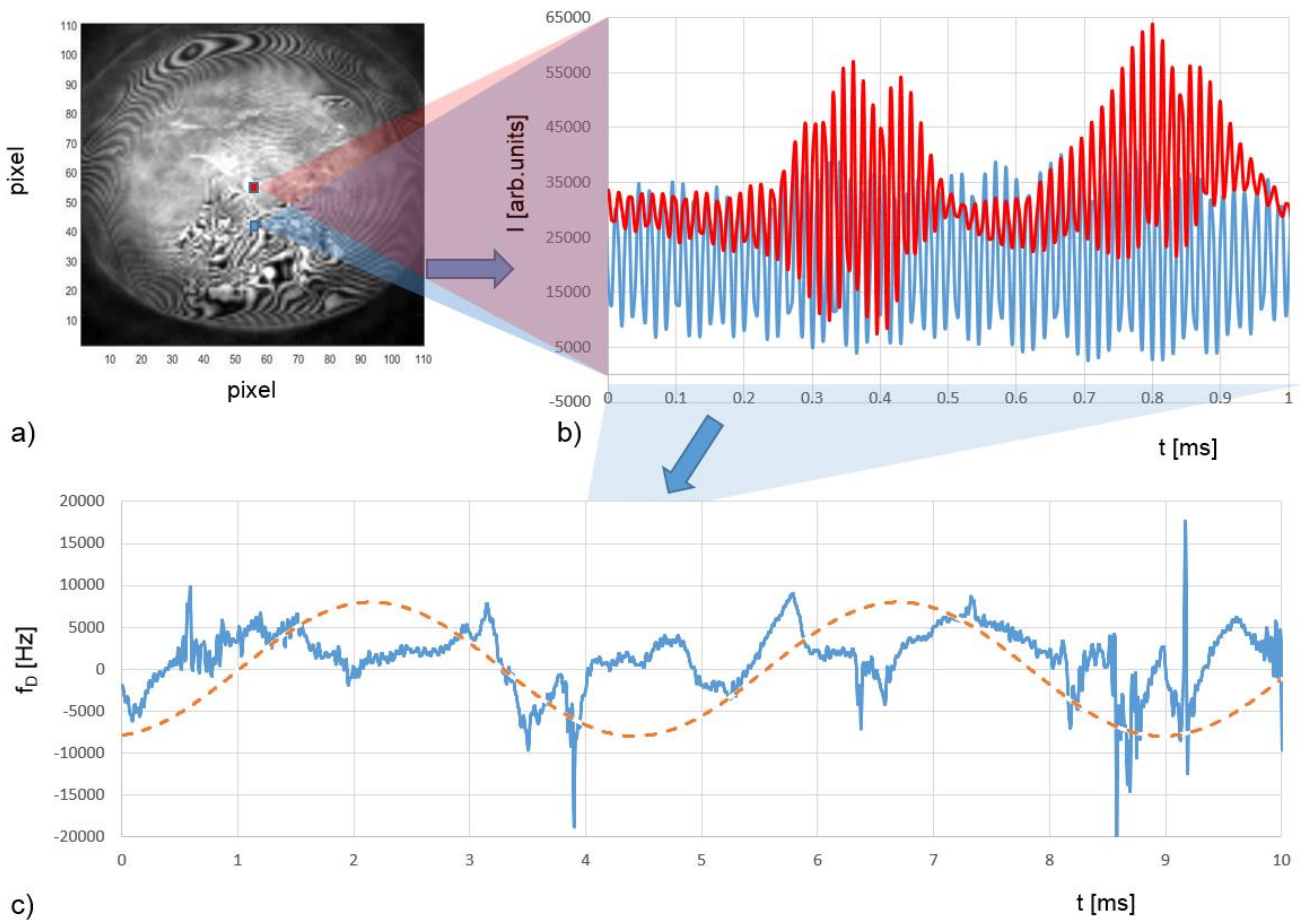


**Fig. 2:** a) Interferogram recorded by the high-speed camera (200kHz frame rate). b) Time signals for two pixels (55/55 and 55/40) with the signal at 60kHz carrier frequency  $f_B$  modulated by the Doppler frequency  $f_D$ . c) Temporal change of the Doppler frequency  $f_D$ . c) is obtained from b) by demodulation and carrier frequency subtraction. The dotted line presents the 225Hz siren signal. Higher harmonics are clearly visible.

#### 4. Experimental setup and data reduction

The CLIV is used to record the Flame Transfer Function (FTF) from a swirl-stabilized flame shown in Fig. 3. Fig. 3a plots a cross-sectional cut of the swirl-stabilized Methane-fired burner operated under atmospheric conditions at a thermal power of 3.44 kW with an equivalence ratio  $\phi$  (Fuel to air ratio) of 0.7. Methane was injected into the air feed line far upstream the burner to ensure perfectly premixed conditions. A siren modulated the air/Methane flow at given frequencies to improve the signal-to-noise ratio when detecting heat release fluctuations. The tangential air/fuel mixture entered the axial flow through 32 cylindrical bores aligned tangentially. According to the definition given by Candel et al. 2014, the tangential flow generated a swirl number of 0.52.

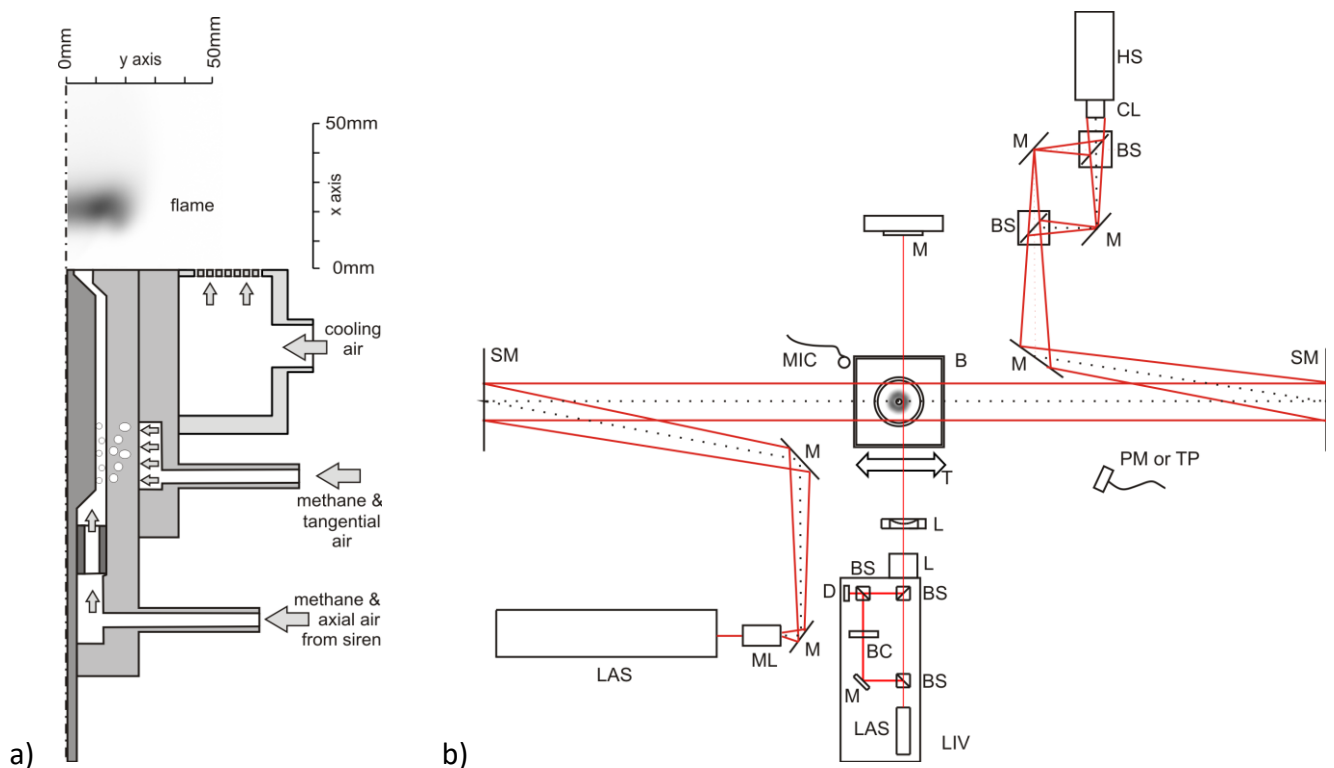


**Fig. 3:** experimental setup. a) burner geometry and dimensions. The swirl-stabilized Methane-fired flame was operated under atmospheric conditions with 0.424g/s axial air flow, 0.397g/s tangential air flow, 0.969g/s cooling air and 0.068g/s Methane mass flow, with the Methane perfectly premixed to the axial and tangential air. (thermal power of 3.44 kW). The axial air was modulated by a siren. b) experimental setup without the CLIV. B burner, LIV commercial single-beam LIV as reference, MIC microphone, PM photomultiplier with band-pass filter for OH\* chemiluminescence, TP thermopile, LAS He-Ne laser, M mirrors, BC Bragg-cell (AOM), D detector, BS beam splitter, CL camera lens, HS high-speed camera, SM spherical mirrors (for shearography).

For reference purposes, a commercially available single-beam LIV was used. (interferometer head OFV-503, velocity decoder VD-06, controller OFV-5000, Polytec, the signal bandwidth chosen was 0 to 100kHz, minimum velocity detected was 0.01m/s, measurement range was 2mm/s/V). The laser beam from the interferometer head was collimated to a diameter of 2mm by a lens with -40mm focal length and reflected by a surface mirror with a size of 300x200mm, glued on a steel block (see Fig. 3b).

As reference for the heat release fluctuations recorded by the full-field LIV, OH\* chemiluminescence data were recorded by a photomultiplier (photomultiplier PMM01, Thorlabs Inc.) with a 310nm band-pass filter (310±3nm CWL, FWHM 10±2nm Bandwidth, 18% Transmission, Edmund Optics). A microphone signal was also permanently detected by a miniature electret condenser microphone (KECG2738PBJ-A, Kingstate Electronics Corp.). Both microphone and photomultiplier were traversed with the flame to keep them in the same position relative to the flame. All signals were referenced by the siren.

The shearography used to record the density (temperature) distribution in the flame used a 20mW He-Ne laser (NEC) two spherical mirrors (2034mm focal length) and a small Mach-Zehnder interferometer instead of the Schlieren stop. This interferometer shears the wave front against itself and provides adjustable sensitivity and carrier fringe patterns. Details of the system are given by Pretzler et al. (1993).

To estimate the heat flux by radiation needed to estimate the loss term in eq. 1, a freshly calibrated thermopile was used (CA2, 0.2-50µm, 19.1µV/W/m<sup>2</sup>, Kipp&Zonen).

Since the determination of a FTF needs the relative oscillations of the burner exit velocity in addition to the relative variations in the heat release rate as functions of frequency, a Constant Temperature Anemometer (CTA) was needed. Here, we used a StreamLine Pro system with a triple fiber probe and scanned closely above the burner exit. (StreamLine Pro triple fiber probe and controller, and StreamLine Pro Automatic Calibrator, DANTEC).

After demodulation of the Doppler frequency from the CLIV pixel signals by means of a QDT, the 27s long time signal was subjected to a digital Fast Fourier Transform (FFT). To do so, we used the pwelch algorithm of MatLab with rectangular (standard) window function and a sample length (SL) of 200000 samples together with a sample rate (SR) of 200000 S/s resulting in a frequency resolution of 1Hz. The averaged power spectra  $\overline{P(f)}$  are then plotted:

$$\overline{P(f)} = \overline{|FFT(f)|^2} \quad (12)$$

After calculating the amplitude of the oscillations for each frequency from eq. 12, the phase of the signal for each position and frequency was obtained from a correlation  $\overline{C_{12}(f)}$  of two signals (cpsd function in MatLab). As a second reference signal, the siren signal was used, although the signals

from photomultiplier, microphone or another pixel could also serve as reference. With the asterix denoting the complex conjugate such a correlation is given by

$$\overline{C_{12}(f)} = \overline{FFT_1^*(f) \cdot FFT_2(f)} \quad (13)$$

The FTF is defined by (Candel et al. 2014):

$$FTF(f) = \frac{\left(\frac{\tilde{Q}(f)}{\bar{Q}}\right)}{\left(\frac{\tilde{v}(f)}{\bar{v}}\right)} \quad (14)$$

In this equation,  $\bar{Q}$  is the global heat release resulting from the Methane mass flow and assuming complete combustion.  $\tilde{Q}(f)$  is the amplitude of the alternating component of heat release rate at a given frequency resulting from eqs. 5 and 10.  $\bar{v}$  and  $\tilde{v}(f)$  are the mean velocities and alternating component of velocity at given frequency  $f$  at the burner exit recorded by CTA. In the same way we define the alternating components of the line-of-sight heat release fluctuation rate as  $\tilde{q}_{f,x,y}$  using the definition of a phase-averaged heat release rate  $\langle \dot{q} \rangle_{f,x,y} = \bar{q}_{f,x,y} + \tilde{q}_{f,x,y} \cos(\varphi_{x,y})$ , with  $f$  the frequency selected by the siren,  $x, y$  the position in the image plane. The value  $\tilde{q}_{f,x,y}$  is the resulting alternating amplitude from the FFT spectra at frequency  $f$  in scanning position  $x, y$  and comes together with the local phase  $\varphi_{x,y}$  (relative to the siren trigger) from the complex FFT spectra.

## 5 Results and Discussion

### 5.1 Comparison between LIV and CLIV data

To verify the proper function of the CLIV, first results were compared to the signal from a single beam LIV for the same sampling rate and data evaluation. In Fig. 4 the amplitude spectra of the Doppler frequency of the CLIV and the commercially available single-beam LIV are compared. Due to the different sampling areas ( $0.47 \times 0.47 \text{mm}^2$  for the CLIV and 2mm beam diameter for the LIV) the signal height is slightly different indicating small scale oscillations below the 2mm resolution, which integrate out when the complex sum of all pixel values is calculated to obtain the global  $\tilde{Q}(f)$  for each frequency. Both systems also provide similar noise levels in the frequency range up to 1kHz (see also Gürtler et al. 2017).

Fig. 5 compares the recordings by LIV and CLIV. While the single-beam commercial LIV scans the half-plane for 10 hours with a  $2 \times 2 \text{mm}^2$  resolution the CLIV recording lasts for 27s with a  $0.47 \times 0.47 \text{mm}^2$  resolution. Finally, Fig. 6 plots the real part of the complex fluctuations of heat release rate,  $\tilde{q}_{f,x,y} \cos(\varphi_{x,y} + \Delta\varphi)$  for four (global) phase steps  $\Delta\varphi$  and siren excitation at  $f=225\text{Hz}$ .

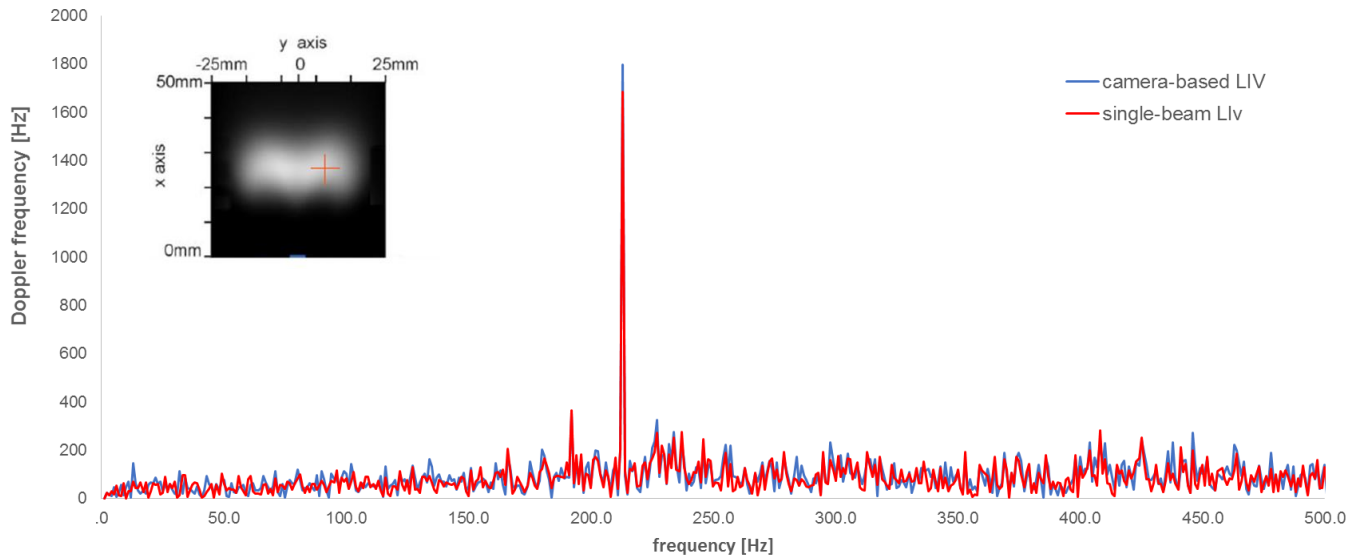


**Fig. 4:** Comparison of the Doppler frequency (amplitude spectrum) recorded by the CLIV (blue) and the single-beam commercial LIV (red) in the relevant frequency range between 0 and 500Hz for a position slightly underneath the flame center (see insert) and a siren excitation at 212Hz. The insert is a long-time exposure, photographic image of the swirl stabilized flame without siren excitation. The different signal height is due to the different sampling areas ( $0.47 \times 0.47 \text{ mm}^2$  for the CLIV and 2mm beam diameter for the LIV) and small scale oscillations.

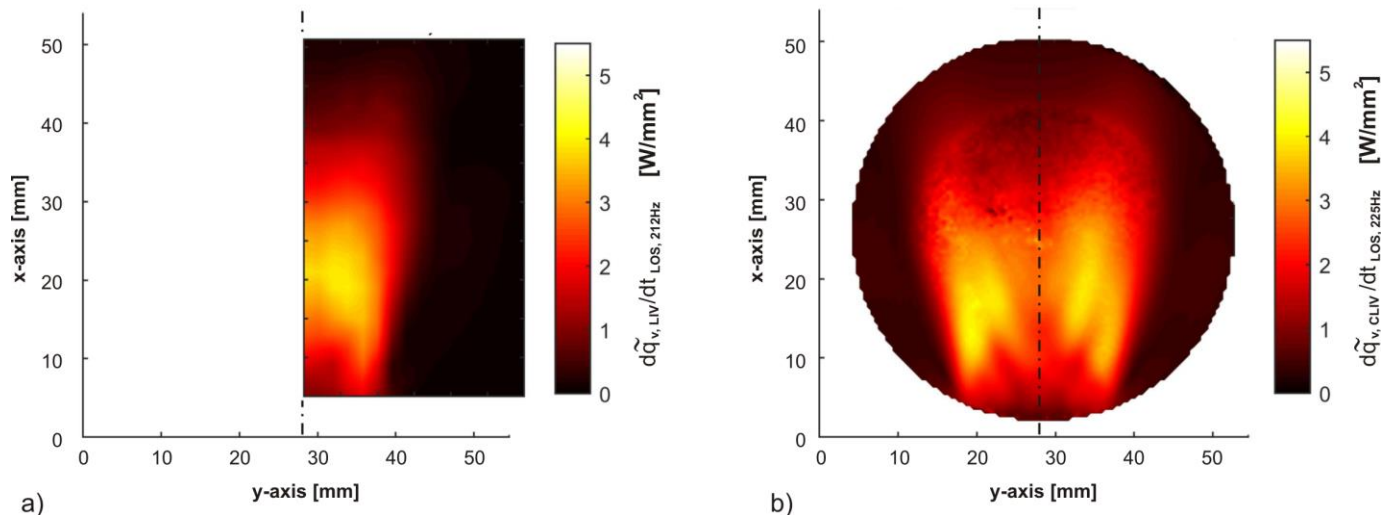


**Fig. 5:** Comparison between a) single-beam commercial LIV and b) CLIV recordings. The field in a) was plotted for the 212Hz excitation frequency and with  $2 \times 2 \text{ mm}^2$  spatial resolution. The scan lasted for 10 hours. The field in b) has a  $0.47 \times 0.47 \text{ mm}^2$  resolution with a recording time of 27s. The excitation frequency was 225Hz. All data are Line-Of-Sight (LOS) data. The lower resolution in a) acts as low-pass filter to the result.



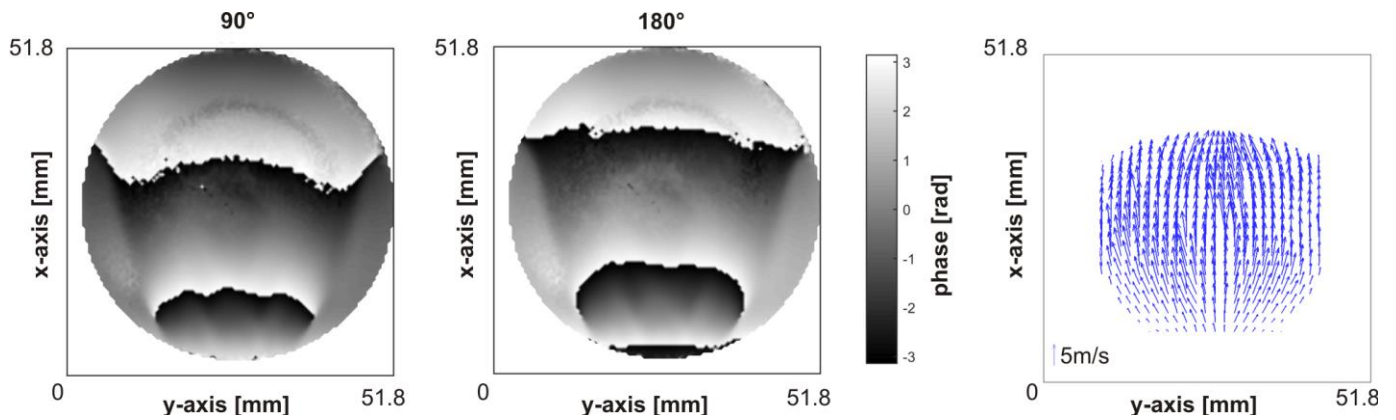


Fig. 7: Plots of two phase maps  $90^\circ$  apart for  $f=225\text{Hz}$ . From these two phase plots a LOS averaged velocity of the heat release fluctuation propagating through the flame can be calculated. We used an adaptive correlation in forward direction. The velocities and fluctuations at this frequency match well with the CTA and previous LDA recordings.

## 5.2 The Flame Transfer Function

The time signal for the CLIV results in Fig.6 and Fig.7 was sampled for 27s and evaluated for a siren frequency of 225cycles/s, meaning that the LOS alternating amplitudes  $\tilde{q}_{225\text{Hz},x,y}$  are a phase average on 6075 cycles. But, the CLIV can also provide instantaneous data. To present these data also, we plotted a time series of raw data in Fig. 8. ( $f_c+f_b$ ; with  $f_c = 60\text{kHz}$ ). Fig. 8 shows 20 instantaneous time frames for one cycle at 225Hz (with siren excitation at this frequency). Assuming a 95% confidence interval and a 40% turbulence level we end up with an error estimate of  $\pm 2\%$  for 6000samples in the phase averaged data.

In order to plot the FTF, first the heat release fluctuations were calculated using eqs. 5 and 10, with the mean density distribution field from shearography  $\bar{\rho}(x, y)$  (or a mean density value  $\bar{\rho} = 0.4 \text{ kg/m}^3$ ) and the corresponding average values for kappa  $\bar{\kappa} = 1.3605$ ,  $\bar{G} = 2.5 \cdot 10^{-4} \text{ m}^3/\text{kg}$  (for hot combustion products and reactants at  $\Phi = 0.7$ ) and  $\bar{p}$  in the combustion zone. The wavelength  $\lambda$  of the CLIV laser is 532nm, the LIV laser and the He-Ne laser used for shearography had 632.9 nm. The complex LOS fluctuations in the field were then summed up for each frequency, to calculate the global amplitude  $\tilde{Q}(f)$  at this frequency as the magnitude from the complex vector.  $\tilde{Q}$  for eq. 14 resulted from the Methane mass flow. The mean velocities and its fluctuations at the single frequencies were recorded by the CTA system.

To obtain a measure of the trustworthiness of the CLIV data, integral brightness fluctuations at the frequencies of the OH\* emissions were recorded using a photomultiplier (PM), as in earlier measurements (Peterleithner et al. 2016b). The fluctuations were referenced to the mean brightness value. For perfectly premixed flames the results of PM and CLIV should match.

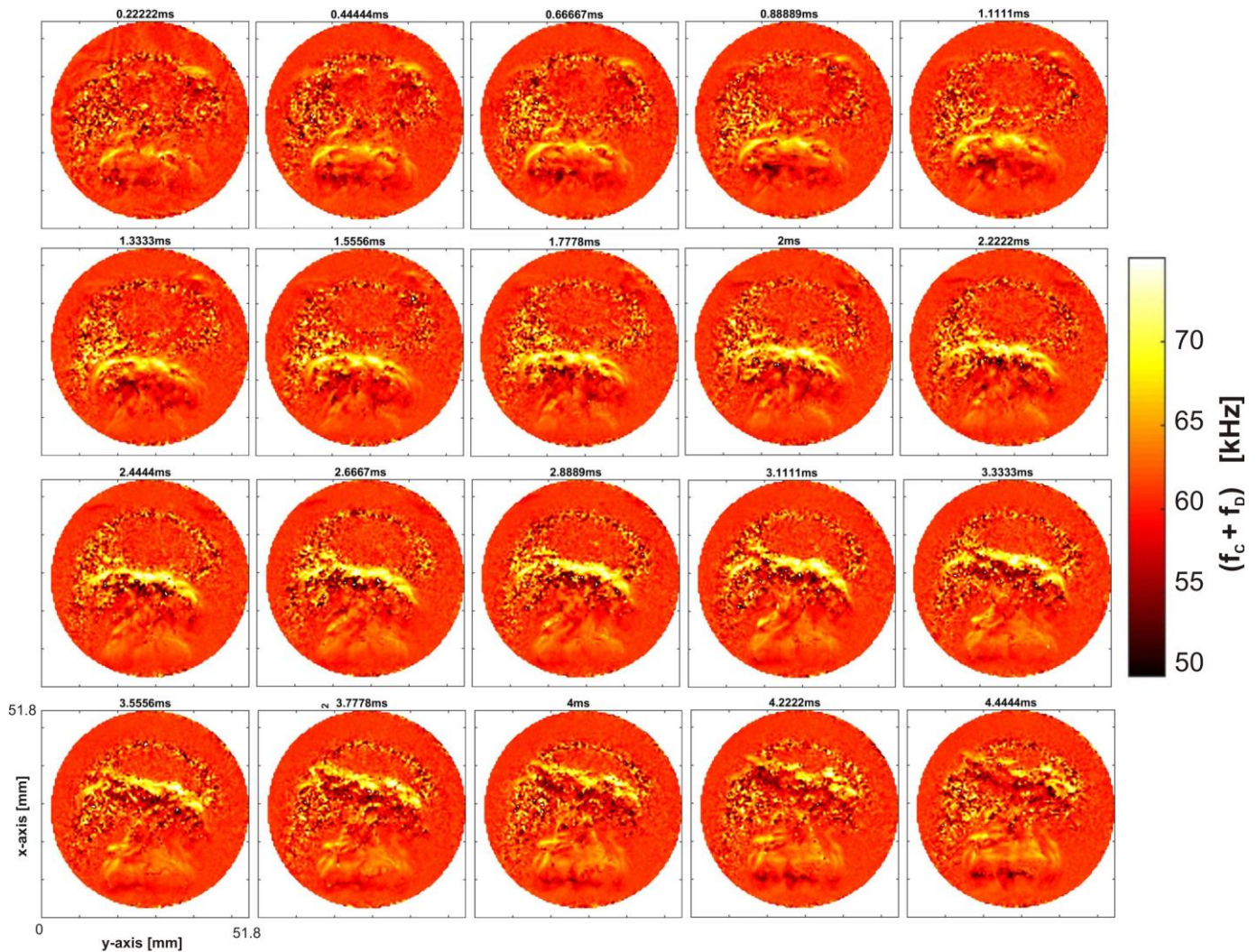


**Fig. 8:** 20 instantaneous time frames of one cycle at 225Hz (siren excitation). Plotted are the raw signals before carrier frequency subtraction ( $f_c=60\text{kHz}$ ) and filtering.

Fig. 9 plots the FTF for frequencies up to 600Hz. For 6 frequencies the local fluctuations are also plotted. On the one side, the flame acts as low-pass filter to incoming fluctuations of pressure or velocity. This can be nicely seen at frequencies above 400Hz, where the correlation between siren excitation and fluctuation in heat release fluctuation is lost. On the other hand, the flame can be viewed as oscillating acoustic dipole in the far field. This becomes evident when discussing the low frequency oscillations. At these frequencies a clear correlation between the local oscillations in heat release rate is given, but since the flow velocity (5-6m/s) is small compared to the speed of sound the flame can be viewed as monopole source to the sound emission. A good example are the oscillations at 300 or 325Hz, where the oscillation amplitudes are strong within the single nodes and antinodes, but overall, cancel out.

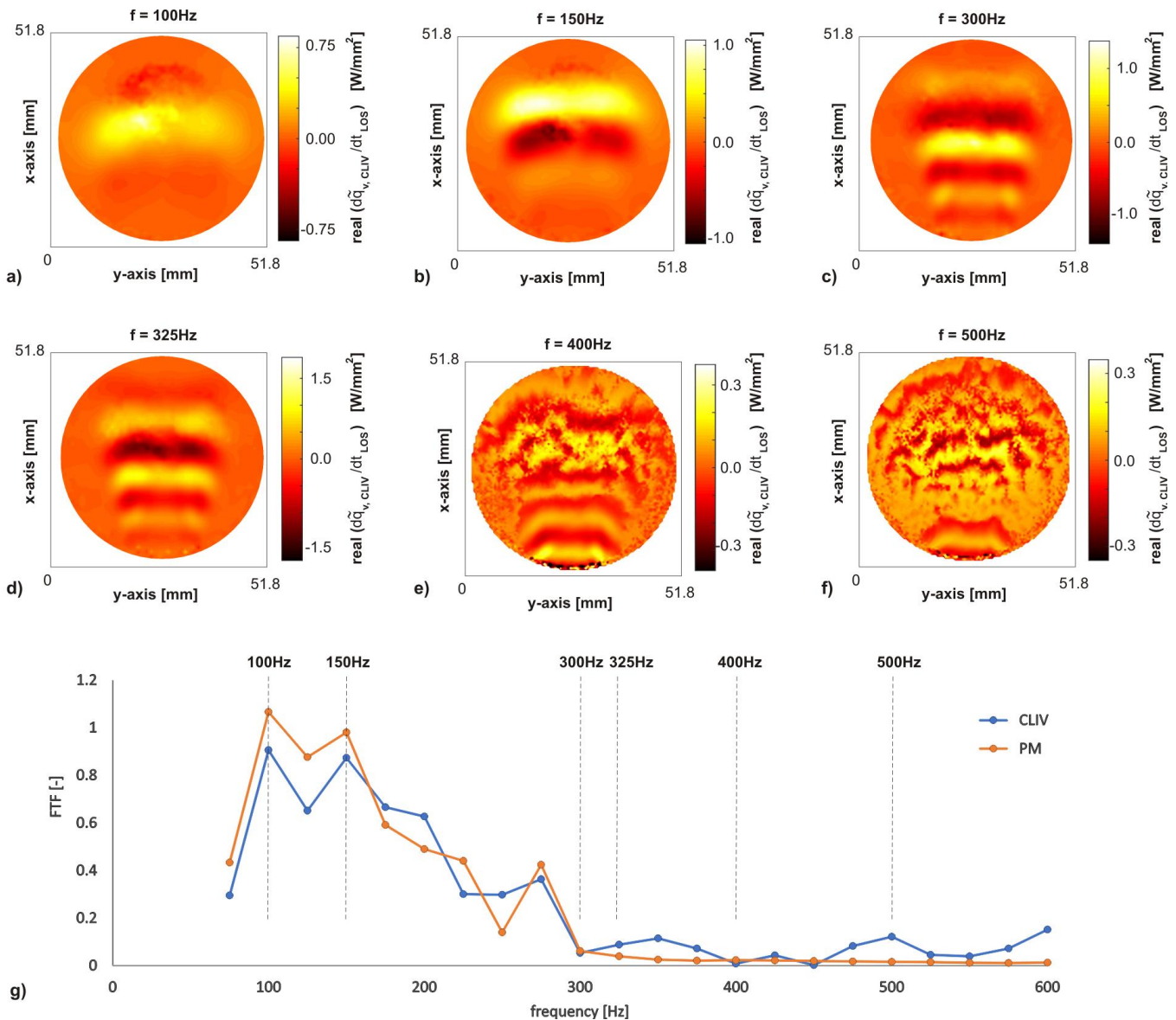


**Fig. 9:** Figures a) to f) show the LOS heat release fluctuation rate of the swirl stabilized flame under atmospheric conditions (swirl number 0.52). The flame was operated at a power of 3.44kW and fired with Methane. The equivalence ratio was 0.7, the reactants perfectly premixed. Figure g) gives the Flame Transfer Function (FTF). The CLIV global data are compared to the global intensity fluctuations recorded by the photomultiplier (PM). The photomultiplier recorded the global chemiluminescence emission from OH\*. The flame acts as a low-pass filter for the incoming flow oscillations superimposed by the siren. Starting at about 400Hz, the correlation between oscillations from the siren and oscillations in the heat release rate is more or less lost.

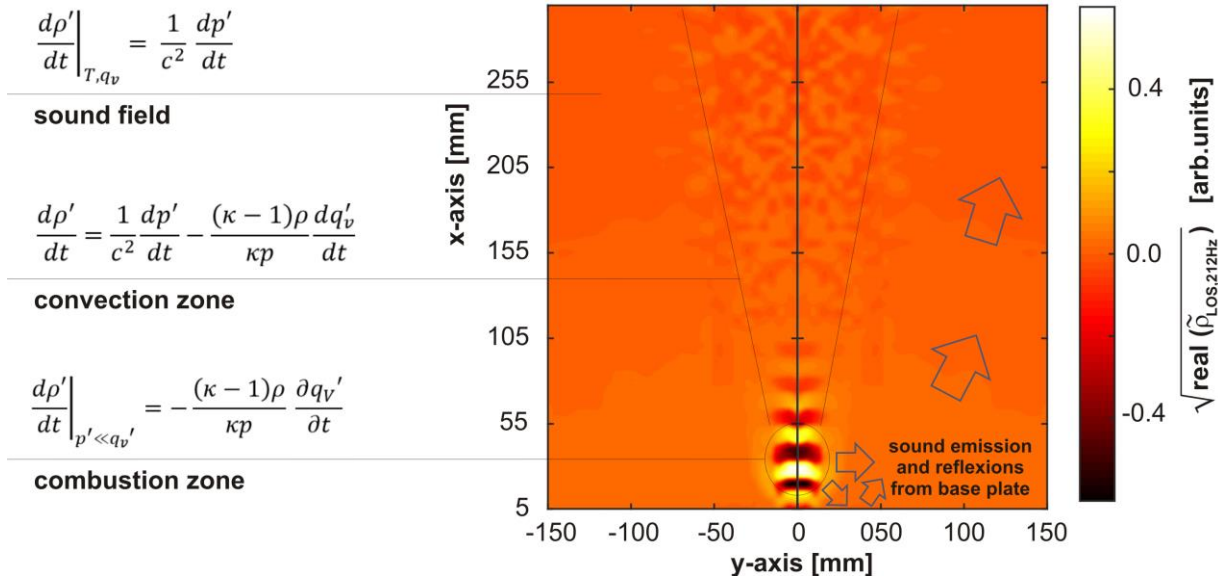


**Fig. 10:** Sound field emitted from the flame oscillating at 212Hz. The combustion zone, the convection zone and the sound field are clearly visible. Pressure waves are emitted from the flame acting as acoustic monopole. These acoustic waves are partially reflected by the base plate of the burner underneath the flame and are slightly refracted in the temperature field around the flame.

Finally, the sound emission of the swirl stabilized flame is discussed in Fig. 10, with the flame excited by the siren at 212Hz. Fig. 10 also discusses the different contributions to density. The strongest density fluctuations are observed in the combustion zone, caused by the fluctuations in heat release. The overall oscillations (monopole assumption) are strong enough to be origin for a sound wave at this frequency.

On the one hand there is a strong emission in horizontal direction, but a significant pressure wave is emitted downwards to the base plate of the burner underneath the flame (see also Fig. 3a). This part is then reflected upwards and refracted towards the flame. These wave reflections contribute to a peak in sound power in the upwards direction and is often found in pressure measurements. It is inclined about  $60^\circ$  towards the base plate and strongly oscillating in angle (Greiffenhagen et al. 2017). Fig. 10 also show the complex influence of pressure and heat fluctuations in the convection zone. These two contributions to density can only be separated by the different wavelength of the distortions.

## 6. Conclusion and outlook

The application of CLIV to flame diagnostics was discussed in this paper. It is a fast way to detect global and local fluctuations in heat release rate in order to identify critical combustion regions. Similar to  $\text{OH}^*$  chemiluminescence it is a line-of-sight method, meaning that for local data

tomographic reconstruction or Abel transform (axial symmetry) are needed. While only global data is needed to record a FTF, the local LOS data can provide valuable clues to the behavior of the flame at certain frequencies. Data are sampled within seconds for each frequency, with the possibility to observe instantaneous flow processes. LIV and CLIV also enable a detailed analysis of the sound emission from the flame at certain frequencies a possibility not provided by chemiluminescence. These abilities of CLIV open new ground in the high speed and real-time observation of feedback control of combustion instabilities with closed-loop systems.

## Acknowledgements

This project is a Lead-Agency D-A-CH project in cooperation between Graz University of Technology, Austria and Technische Universität Dresden, Germany, and was funded by the Austrian Science Fund FWF within Grant No. FWF-I2544-N30 and by the German Research Foundation DFG within project DFG CZ 55/33-1. We also thank Mr. Heiko Scholz for supporting us during the first CLIV measurements.

## References

- Balachandran R, Ayoola BO, Kaminski C, Dowling AP, Mastorakos E (2005) Experimental investigation of the nonlinear response of turbulent premixed flames to imposed inlet velocity oscillations, *Combustion and Flame*, vol. 143, pp. 37-55.
- Candel S, Durox D, Schuller T, Bourgooin J, Moeck JP (2014) Dynamics of swirling flames, *Annu. Rev. Fluid Mech*, vol. 46, 147-173
- Crighton DG, Dowling AP, Williams JEF, Heckl MA, Leppington FA (1992) *Modern Methods in Analytical Acoustics: Lecture Notes*, Springer Verlag, Berlin Heidelberg, ISBN 987-3-540-19737-9
- Dowling AP, Mahmoudi Y, (2015) Combustion noise, *Proceedings of the Combustion Institute*, vol. 35, pp. 65-100
- Gardiner WC, Hidaka Y, Tanzawa Y (1981) Refractivity of Combustion Gases, *Combustion and Flame*, vol. 40, pp. 213-219
- Giuliani F, Wagner B, Woisetschläger J, Heitmeir F (2006) Laser vibrometry for real-time combustion instability diagnostics, *Proc. ASME Turbo Expo*, GT GT2006-90413
- Greiffenhagen F, Peterleithner J, Woisetschläger J (2017) Prediction of Combustion Noise from a Swirl-Stabilized Flame using Laser-Interferometric-Vibrometry validated by Acoustic Measurements, *Proceedings ASME Turbo Expo*, GT2017-63418
- Greiffenhagen F, Peterleithner J, Gürtler J, Fischer A, Woisetschläger J, Czarske J (2018) "Quantitative measurement and estimation of uncertainties of heat release fluctuations in swirl stabilized flames with laser interferometric vibrometry," *Combustion and Flame*, under review

- Gren P, Tatar K, Granström J, Molin N-E, Jansson EV (2006) Laser vibrometry measurements of vibration and sound fields of a bowed violin, *Measurement Science and Technology*, vol. 17, pp. 635-644, 2006
- Gürtler J, Greiffenhagen F, Peterleithner J., Woisetschläger J, Haufe D, Fischer A, Czarske J (2016) Seedingless measurement of the heat release rate and the velocity in swirlstabilized flames using camera-based laser-vibrometry, *Proc. Fachtagung Experimentelle Strömungsmechanik*, 6. – 8. September 2016, Cottbus
- Gürtler J, Greiffenhagen F, Woisetschläger J, Haufe D, Czarske J (2017) Non-invasive seedingless measurements of the flame transfer function using high-speed camera-based laser vibrometry, *Proc. SPIE* 10329, 26 June 2017
- Lauer MRW, (2011) Determination of the Heat Release Distribution in Turbulent Flames by Chemiluminescence Imaging, Dissertation, Technische Universität München, pp. 147-173
- Lewin AC (1998) Compact laser vibrometer for industrial and medical applications, *Proc. SPIE*, vol. 3411, pp. 61-67
- Leitgeb T, Schuller T, Durox D, Giuliani F, Köberl S, Woisetschläger J (2013) Interferometric determination of heat release rate in a pulsated flame, *Combustion and Flame*, vol. 160, pp. 589-600
- Lieuwen TC (2012) *Unsteady combustor physics*, pp. XIX, 405, Cambridge Univ. Press, Cambridge, ISBN 978-1-107-01599-9
- Martarelli M, Castellini P, Tomasini EP (2013) Subsonic jet pressure fluctuation characterization by tomographic laser interferometry, *Exp Fluids* 54 (2013) 1626 (13 pp)
- Mayrhofer N, Woisetschläger J (2001) Frequency analysis of turbulent compressible flows by laser vibrometry, *Experiments in Fluids*, vol. 21, pp. 153-161
- Merzkirch W (1987) *Flow Visualization*, 2 ed., Academic Press Inc., Orlando, ISBN 0-12-491351-2
- Peterleithner J, Woisetschläger J (2015) Laser vibrometry for combustion diagnostics in thermoacoustic research, *Technisches Messen*, vol. 82, pp. 549-555, 2015
- Peterleithner J, Stadlmair NV, Woisetschläger J, Sattelmayer T (2016a) Analysis of measured flame transfer functions with locally resolved density fluctuation and OH-Chemiluminescence Data, *Journal of Engineering for Gas Turbines and Power*, vol. 138, 2016.
- Peterleithner J, Basso R, Heitmeir F, Woisetschläger J, Schlußler R, Czarske J, Fischer A (2016b) Comparison of flame transfer functions acquired by chemiluminescence and density fluctuation, *Proceedings of the ASME Turbo Expo GT2016-57485*
- Pretzler G, Jäger H, Neger T (1993) High-accuracy differential interferometry for the investigation of phase objects, *Meas Sci Technol* 4, 649-658
- Pretzler G, Jäger H., Neger T, Philipp H, Woisetschläger J (1992) Comparison of different methods of Abel inversion using computer simulated and experimental side-on data, *Z. Naturforsch.*, Vol. 47a, 955-970

- Selbach H, Lewin AC, Roth V (1992) Laser Doppler Vibrometer for applications in the automotive industry, Proc. 25th ISATA Silver Jubil. Int. Symp. Automot. Technol. Autom., Florence, pp. 217–224
- Strahle WC (1971) On combustion generated noise, Journal of Fluid Mechanics, vol. 49, no. 02, pp. 399-414
- Williams FA (1994) Combustion Theory, 2nd Edition, Perseus Books, Reading, Massachusetts, ISBN 0-8053-9801-5
- Zipser L, Lindner S, Behrendt R (2002) Interferometric Measurement and Visualisation of Acoustic Waves and Vortexes, vol. 69, pp. 275-281